Quantum Hall Effect and Disorder: Topological Properties

Ye Yong'En, Joash

Supervisors:

A/Prof Benoît Grémaud

Prof Christian Miniatura

In Collaboration with Dr Vincent Sacksteder IV, NTU

Abstract

Whenever the Fermi energy lies in a mobility gap, the Hall conductivity of a 2D system is quantized and is equal to the Chern number multiplied by the conductance quantum. Due to bulk-edge correspondence, the Chern number is also equivalent to the number of edge-states present at Fermi energy.
Typically, finding the Chern number of large disordered systems is done indirectly through conductance calculations, as direct calculation of the Chern number by definition requires full diagonalization of the system Hamiltonian. In this project we hoped to obtain some characterization of the systems conduction properties by studying a different variable that is local in energy, and hence only require some of the states near the Fermi energy. Unfortunately, the proposed variable seems unable to describe the system Chern number, and is to some extent, its properties are easily explained, yielding a negative result.

Acknowledgments

I would like to thank both my supervisors, A/Prof Benoît Grémaud and Prof Christian Miniatura for their guidance during the course of the project, and their patience for dealing with someone who started with very little knowledge of this field of physics. When I first started working on the project at the beginning of the academic year, I knew nearly nothing about solid state and condensed matter physics, Berry phase in electronic properties, conduction, disorder and other sub-fields of physics that should be 'standard' for someone working in this area. In particular, I am especially grateful for our weekly meetings where I would have a chance to discuss my doubts and review certain ideas from papers that I came across during the week. These weekly discussions have been an essential part in improving my understanding of the subject. Equally important, I learned that dealing with negative results is simply a part of research, and it is the knowledge gained through the process that matters.
I would also like to thank Dr Vincent Sacksteder IV, who came up with the initial idea for the project, for numerous discussions we had.

Contents

Chapter 1

Introduction

A large part of physics is about categorizing things. The full state of a system is in general, complicated to specify. Classically, we would need to track every single particle in the system and its momentum. Quantum mechanically, we would need to write down its decomposition in terms of the eigenstates of the system Hamiltonian. Instead of dealing with properties at such a detailed level, we look for similarities between states and group them accordingly. These groups we call *phases* and states in different phases are sufficiently different such that to transform one state to another would require a *phase transition*; a phase is robust against small perturbations.

In the integer quantum Hall effect, described by non-interacting particle theory, the quantized Hall conductivity defines different phases of conduction. Each phase is characterized by a topological index called the *Chern number*. The fact that the Chern number describes a phase means that the transition between phases requires a phase transition, and this implies that small perturbations, for example by a random disordered potential, will not change the conduction properties of a system, that is, the perturbed system and the original system are described by the same phase.

The calculation of the Chern number, is in general, not something that can be done practically on a computer for large systems. Generally, to show that a system is in a particular topological phase, numerical simulation of conduction or measurements are performed, and if the conduction is quantized, then the system is in a topological phase. Instead, we propose to study a different variable that we call Q matrices, in hope of having a different way of obtaining the conduction properties of a system, or at least providing a different perspective. Unfortunately, it seems that such a variable is too simple for describing these topological phases, and hence we only obtain a negative result.

The report is organized as follows. Chapter 2 reviews known ideas regarding the Chern number and its relation to the Hall conductivity and the edge states that show up when finite boundaries are imposed. Chapter 3 briefly covers the numerical models used as well as disordered potential models. Chapter 4 is on the results regarding the Q matrices for one particular model of a system with non vanishing topological number. The section ends with a discussion of the results and why we think the Q matrix variables may not be useful. Finally, we conclude in Chapter 5 with a short discussion on the problems with defining such a variable.

Chapter 2

Background

2.1 Disorder and Localization in 2D

The theory of Anderson localization has the following statement about the behavior of electronic wave-functions in the presence of disorder. In 1D or 2D, the conductance always decreases with the system size whenever a random potential (randomly spaced scatterers, for example) is present. In 3D, there is a critical 'randomness strength' beyond which a system would become insulting in the infinite size limit, or remain a conductor. Fig. 2.1 shows the so-called β function for the different dimensions. The β function is defined as

$$\beta = L\frac{\mathrm{d}\ln g}{\mathrm{d}L} \tag{2.1}$$

which describes the behavior of the dimensionless conductance $g = \frac{T}{1-T}$, T being the transmission coefficient, as the system size L increases. Scaling arguments lead to the behavior shown in Fig. 2.1. The main point is that randomness/disorder causes electronic states to localize in 2D or less.
However, we will be describing topological materials (in 2D) where conducting states exist that are robust against disorder. These states are said to be 'topologically protected' and hence resist localization by disorder.

2.2 Hall Conductivity: Linear Response to an Electric Field

Suppose a system described by some Hamiltonian H currently in the ground state $|\psi_0\rangle$ is subject to an electric field perturbation along the y direction. We write the total Hamiltonian as

$$\begin{aligned} H_E &= H + V \\ &= H - eEy \end{aligned}$$

The new ground state $|\psi_{0,E}\rangle$ can be calculated to first order using standard perturbation theory in terms of the eigenstates of H denoted by $|\psi_n\rangle$

$$|\psi_{0,E}\rangle = |\psi_0\rangle + \sum_{n>0} \frac{\langle\psi_n|\,(-eEy)\,|\psi_0\rangle}{E_0 - E_n}\,|\psi_n\rangle \tag{2.2}$$

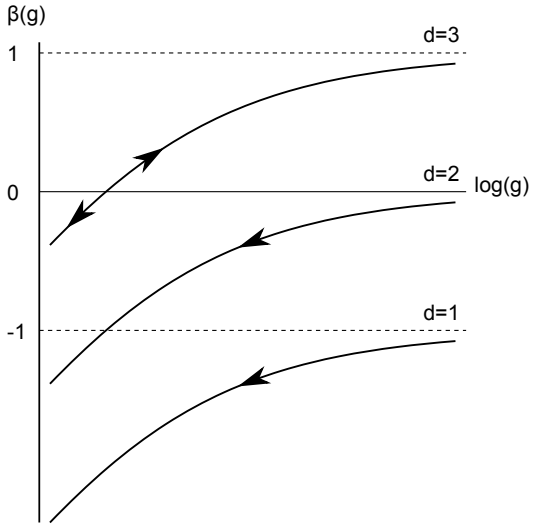

Figure 2.1: β Function for $d = 1, 2, 3$. Arrows indicate the change in conductance as the system size is increased. In $d < 2$, it is always negative.

We can then calculate the expectation of the current density along the x direction to first order in the electric field

$$\begin{aligned}\langle\psi_{0,E}|\, j_x\, |\psi_{0,E}\rangle &= \sum_{n>0} \frac{\langle\psi_n|\,(-eEy)\,|\psi_0\rangle\,\langle\psi_0|\, j_x\,|\psi_n\rangle + \langle\psi_0|\,(-eEy)\,|\psi_n\rangle\,\langle\psi_n|\, j_x\,|\psi_0\rangle}{E_0 - E_n} \\ &\quad + \langle\psi_0|\, j_x\,|\psi_0\rangle + O\left(E^2\right) \end{aligned} \tag{2.3}$$

In 2D, $j_i = -\frac{e}{A} v_i = \frac{i}{\hbar}\,[H, x_i]$, where A is the area of the system. Using this relation, we express the matrix elements of y in terms of v_y to obtain

$$\Delta j_x \equiv \langle\psi_{0,E}|\, j_x\,|\psi_{0,E}\rangle - \langle\psi_0|\, j_x\,|\psi_0\rangle \tag{2.4}$$

$$\Delta j_x = E\frac{ie^2\hbar}{A}\sum_{n>0} \frac{\langle\psi_n|\, v_y\,|\psi_0\rangle\,\langle\psi_0|\, v_x\,|\psi_n\rangle - \langle\psi_0|\, v_y\,|\psi_n\rangle\,\langle\psi_n|\, v_x\,|\psi_0\rangle}{\left(E_0 - E_n\right)^2} \tag{2.5}$$

So the Hall conductivity, that is, the response of the current along x direction to an electric field applied along the y direction is given by

$$\begin{aligned}\sigma_{xy} &= \frac{\Delta j_x}{E} \\ &= \frac{ie^2\hbar}{A}\sum_{n>0} \frac{\langle\psi_0|\, v_x\,|\psi_n\rangle\,\langle\psi_n|\, v_y\,|\psi_0\rangle - \langle\psi_0|\, v_y\,|\psi_n\rangle\,\langle\psi_n|\, v_x\,|\psi_0\rangle}{\left(E_0 - E_n\right)^2} \end{aligned} \tag{2.6}$$

This is known as Kubo's formula for the DC Hall conductivity. A more general formula for conductivity at other frequencies can be derived in similar fashion, but is not necessary for our purposes. In the derivation, we assumed the following:

- The ground state is non-degenerate
- The ground state is separated from the first excited state by a finite energy gap

2.3 Hall Conductivity as Topological Invariant: Chern Number

2.3.1 The Flux Trick

We now discuss the so-called 'flux trick' first introduced in [1], which is to define the Hall conductivity in terms of a topological invariant called the Chern number which is an integer.
Consider the family of 2D Hamiltonians with an additional flux parameter $\boldsymbol{\kappa}$ on a presumably large region of dimensions L_x by L_y

$$H(\boldsymbol{\kappa}) = \frac{1}{2m}\sum_i \left(\mathbf{p}_i - e\mathbf{A}(\mathbf{r}_i) + \hbar\boldsymbol{\kappa}\right)^2 + V \tag{2.7}$$

The reason for doing so will become clearer in a moment. The potential V represents in general 1-body (including disorder) or 2-body (interactions) contributions. The many particle velocity operator becomes

$$\begin{aligned}\mathbf{v}(\boldsymbol{\kappa}) &= \frac{1}{m}\sum_i \mathbf{p}_i - e\mathbf{A}(\mathbf{r}_i) + \hbar\boldsymbol{\kappa} \\ &= \frac{1}{\hbar}\frac{\partial H(\boldsymbol{\kappa})}{\partial \boldsymbol{\kappa}}\end{aligned} \tag{2.8}$$

The solution to the time-independent Schrodinger equation in position basis is then a function of all the single particle coordinates; $(\langle\mathbf{r}_1| \otimes \langle\mathbf{r}_2| \otimes ... \otimes \langle\mathbf{r}_N|)\,|\psi\rangle = \psi(\mathbf{r}_1, \mathbf{r}_2, ..., \mathbf{r}_N)$. The presence of the vector potential in general forbids regular periodic boundary conditions. Instead we impose magnetic periodic boundary conditions of the form $\mathcal{T}_{L_x\hat{\mathbf{x}}}|\psi\rangle = |\psi\rangle$, $\mathcal{T}_{L_y\hat{\mathbf{y}}}|\psi\rangle = |\psi\rangle$, where $\mathcal{T}_{\mathbf{a}}$ are magnetic translation operators.

$$\mathcal{T}_{\mathbf{a}} = \exp\left(i\frac{\left(\mathbf{p} + \frac{e}{2}(\mathbf{r}\wedge\mathbf{B})\right)\cdot\mathbf{a}}{\hbar}\right) \tag{2.9}$$

In doing so, we assume that L_x and L_y are large enough that the magnetic flux through the region is a rational number of flux quanta. From now on, whenever we refer to periodic boundary conditions, we mean magnetic periodic boundary conditions if a vector potential is present.
Substituting (2.8) into (2.6) we obtain a $\boldsymbol{\kappa}$ dependent Hall conductivity

$$\sigma_{xy}(\boldsymbol{\kappa}) = \frac{ie^2}{A\hbar}\sum_{n>0}\frac{\langle\psi_0|\frac{\partial H}{\partial\kappa_x}|\psi_n\rangle\langle\psi_n|\frac{\partial H}{\partial\kappa_y}|\psi_0\rangle - \langle\psi_0|\frac{\partial H}{\partial\kappa_y}|\psi_n\rangle\langle\psi_n|\frac{\partial H}{\partial\kappa_x}|\psi_0\rangle}{(E_0 - E_n)^2} \tag{2.10}$$

For brevity we leave out the $\boldsymbol{\kappa}$ dependence of the Hamiltonian, the states and the energy eigenvalues. Using the identities

$$\langle\psi_0|\frac{\partial H}{\partial\boldsymbol{\kappa}}|\psi_n\rangle = (E_0 - E_n)\langle\frac{\partial\psi_0}{\partial\boldsymbol{\kappa}}|\psi_n\rangle \tag{2.11}$$

$$\sum_n |\psi_n\rangle\langle\psi_n| = 1 \tag{2.12}$$

we can rewrite the Hall conductivity as

$$\sigma_{xy}(\boldsymbol{\kappa}) = \frac{ie^2}{A\hbar}\left(\langle\frac{\partial\psi_0}{\partial\kappa_x}|\frac{\partial\psi_0}{\partial\kappa_y}\rangle - \langle\frac{\partial\psi_0}{\partial\kappa_y}|\frac{\partial\psi_0}{\partial\kappa_x}\rangle\right) \tag{2.13}$$

Suppose $|\psi_0(\boldsymbol{\kappa}_0)\rangle$ is the ground state of $H(\boldsymbol{\kappa}_0)$, that is

$$H(\boldsymbol{\kappa}_0)|\psi_0(\boldsymbol{\kappa}_0)\rangle = E_0(\boldsymbol{\kappa}_0)|\psi_0(\boldsymbol{\kappa}_0)\rangle \tag{2.14}$$

and satisfies the boundary conditions. Then while $\exp(-\boldsymbol{\kappa}\cdot\mathbf{R})|\psi_0(\boldsymbol{\kappa}_0)\rangle$ satisfies

$$H(\boldsymbol{\kappa}+\boldsymbol{\kappa}_0)(\exp(-\boldsymbol{\kappa}\cdot\mathbf{R})|\psi_0(\boldsymbol{\kappa}_0)\rangle) = E_0(\boldsymbol{\kappa}_0)(\exp(-\boldsymbol{\kappa}\cdot\mathbf{R})|\psi_0(\boldsymbol{\kappa}_0)\rangle) \tag{2.15}$$

it does not in general satisfy the boundary conditions, except at $\boldsymbol{\kappa} = 2\pi\left(\frac{n}{L_x}\hat{\mathbf{x}} + \frac{m}{L_y}\hat{\mathbf{y}}\right)$. So we notice that the ground state $|\psi_0(\boldsymbol{\kappa})\rangle$ returns to itself up to a phase factor whenever κ_x and κ_y vary by $\frac{2\pi}{L_x}$ and $\frac{2\pi}{L_y}$ respectively. Defining $\theta_x = \kappa_x L_x$, $\theta_y = \kappa_y L_y$ we obtain that $\sigma_{xy}(\theta_x,\theta_y)$ is a periodic function of θ_x and θ_y, i.e. it is a function on the unit torus parametrized by θ_x and θ_y.
Now we consider what happens when $\boldsymbol{\kappa}$ is slowly varied in time. Glancing back at the Hamiltonian (2.7), we see that this corresponds to having a time varying vector potential, i.e. an electric field. In particular, we consider the case where $\hbar\boldsymbol{\kappa}(t) = eEt\hat{\mathbf{y}}$. In the limit of vanishing electric field E, the parameters $\boldsymbol{\kappa}(t)$ vary slowly in time such that the system remains in the ground state of the time dependent Hamiltonian $H(\boldsymbol{\kappa}(t))$ via the adiabatic theorem. Let T be the time interval for φ to vary from 0 to 2π. Then the average current is the total charge transported divided by T. The average conductivity is then the average current divided by the electric field

$$\begin{aligned}\bar{\sigma} &= \frac{1}{E}\frac{1}{T}\int_0^T j_x dt \\ &= \frac{1}{2\pi}\int_0^{2\pi}\sigma(\theta_y)\,d\theta_y\end{aligned} \tag{2.16}$$

So far we have only averaged over one angle. If we were to average over both angles (θ_x,θ_y) then

$$\begin{aligned}\bar{\sigma} &= \frac{1}{4\pi^2}\int_0^{2\pi}\int_0^{2\pi}\frac{ie^2}{\hbar}\langle\frac{\partial\psi_0}{\partial\theta_x}|\frac{\partial\psi_0}{\partial\theta_y}\rangle - \langle\frac{\partial\psi_0}{\partial\theta_y}|\frac{\partial\psi_0}{\partial\theta_x}\rangle\,d\theta_x d\theta_y \\ &= -\frac{e^2}{h}\frac{1}{2\pi i}\int_0^{2\pi}\int_0^{2\pi}\langle\frac{\partial\psi_0}{\partial\theta_x}|\frac{\partial\psi_0}{\partial\theta_y}\rangle - \langle\frac{\partial\psi_0}{\partial\theta_y}|\frac{\partial\psi_0}{\partial\theta_x}\rangle\,d\theta_x d\theta_y \\ &= -\frac{e^2}{h}C\end{aligned} \tag{2.17}$$

where the quantity

$$C = \frac{1}{2\pi i}\int_0^{2\pi}\int_0^{2\pi}\langle\frac{\partial\psi_0}{\partial\theta_x}|\frac{\partial\psi_0}{\partial\theta_y}\rangle - \langle\frac{\partial\psi_0}{\partial\theta_y}|\frac{\partial\psi_0}{\partial\theta_x}\rangle\,d\theta_x d\theta_y \tag{2.18}$$

is an integral of the *Berry Curvature* of the ground state in the parameter space (θ_x,θ_y). It is called the first Chern number and is an integer (the integral of

Berry Curvature over a closed surface is always an integer multiple of 2π. This follows from single valuedness of the wavefunction). It is well defined as long as the assumptions used in the non-degenerate perturbation derivation of the Hall conductivity holds for all (θ_x, θ_y). Berry Curvature is undefined when two energy levels become degenerate.
It will be useful later to write the Chern number in the form

$$\begin{aligned} C &= \frac{1}{2\pi i}\int_0^{2\pi}\int_0^{2\pi} \mathrm{Tr}\left\{P\left[\partial_{\theta_x}P, \partial_{\theta_y}P\right]\right\} d\theta_x d\theta_y \qquad (2.19) \\ P(\theta_x, \theta_y) &= |\psi_0(\theta_x, \theta_y)\rangle \langle\psi_0(\theta_x, \theta_y)| \end{aligned}$$

where $P(\theta_x, \theta_y)$ is the ground state projector.

2.3.2 Non-Interacting Case

Consider the case of non-interacting electrons. Then the many particle Hamiltonian becomes a direct sum of single particle Hamiltonians $h(\theta, \varphi)$. The ground state is then the Slater determinant of lowest energy occupied single particle states.
We can then express then Chern number in (2.19) by simply changing the ground state projector P to the projector onto the N lowest occupied single particle states

$$P(\theta_x, \theta_y) = \sum_{n=1}^{N} |n(\theta_x, \theta_y)\rangle \langle n(\theta_x, \theta_y)| \qquad (2.20)$$

The condition that the many particle ground state be separated from the first excited state by a finite energy gap translates to the Nth single particle state being separated from the $(N+1)$th state by a finite energy gap.

2.3.3 Relation to Brillouin Zone and Crystal Momentum in non-Disordered Systems

Consider now the case where we deal with non-interacting electrons in a periodic potential, that is, the single particle Hamiltonian is given by

$$h = \frac{\mathbf{p}^2}{2m} + V \qquad (2.21)$$

where $V(x, y) = V(x + a, y) = V(x, y + b)$. Bloch's theorem states that a basis for the eigenfunctions of the single particle Hamiltonian are given by

$$|\psi_{n,\mathbf{k}}\rangle = e^{i\mathbf{k}\cdot\mathbf{r}} |u_{n,\mathbf{k}}\rangle \qquad (2.22)$$

where $|u_{n,\mathbf{k}}\rangle$ are periodic functions in position with same periodicity as the potential energy and are solutions of

$$\begin{aligned} h(\mathbf{k})|u_{n,\mathbf{k}}\rangle &= E_{n,\mathbf{k}}|u_{n,\mathbf{k}}\rangle \qquad (2.23) \\ h(\mathbf{k}) &= e^{-i\mathbf{k}\cdot\mathbf{r}} h e^{i\mathbf{k}\cdot\mathbf{r}} \\ &= \frac{(\mathbf{p}+\hbar\mathbf{k})^2}{2m} + V \qquad (2.24) \end{aligned}$$

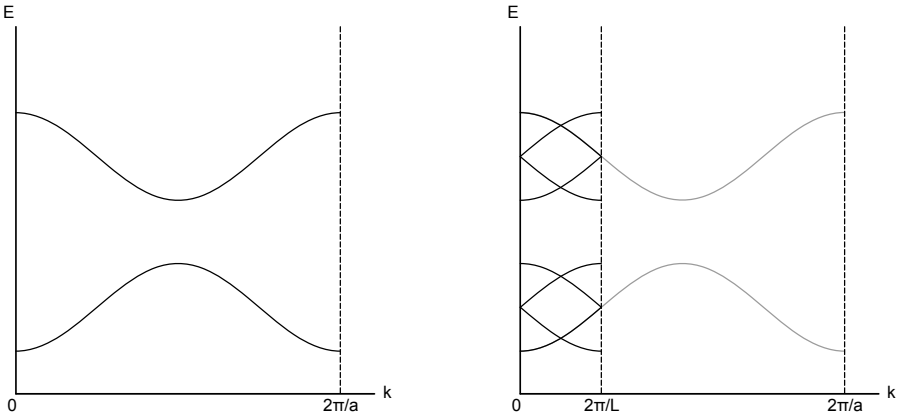

(a) Full Brillouin Zone of size $\frac{2\pi}{a}$, showing 2 bands.

(b) 'Folded' Brillouin Zone of size $\frac{2\pi}{L}$. The 2 bands have been 'folded' to form 8 bands.

Figure 2.2

with periodic boundary conditions $u_{n,\mathbf{k}}(x,y) = u_{n,\mathbf{k}}(x+a,y) = u_{n,\mathbf{k}}(x,y+b)$. The states are labeled by the crystal momentum $\mathbf{k} \in \text{BZ}$, and band index n , where BZ refers to the first Brillouin Zone.
This is similar to the $\boldsymbol{\kappa}$ dependent Hamiltonian introduced earlier without interactions, disorder and magnetic field, except that instead of solving for states periodic over L_x and L_y, we are solving for states periodic over a and b. To see the relation between the two, we notice that solving for eigenstates on the larger unit cell L_x and L_y is simply folding the Brillouin Zone into a smaller region, from $\frac{2\pi}{a}$ by $\frac{2\pi}{b}$ to $\frac{2\pi}{L_x}$ by $\frac{2\pi}{L_y}$. The higher $\mathbf{k}$ states in the full Brillouin Zone show up as states in another band in the folded Brillouin Zone (Fig. 2.2). Hence the projector onto the occupied states is the same for the full Brillouin Zone or the folded Brillouin Zone, that is, the Chern number can be expressed equivalently as an integral over the Brillouin Zone.

$$C = \frac{1}{2\pi i}\int_{BZ} \text{Tr}\left\{P(\mathbf{k})\left[\partial_{k_x}P(\mathbf{k}), \partial_{k_y}P(\mathbf{k})\right]\right\} d\mathbf{k} \tag{2.25}$$

The constraint that the Nth occupied state is separated from the $(N+1)$th state by a finite energy means that the single-particle states are occupied up to the bottom of a band gap in the spectrum, i.e. there are n filled bands, and the nth band is separated from the $(n+1)$th band by a finite energy gap. This is why the Chern number is said to describe the momentum space topology.

2.4 Bulk-Edge Correspondence: Edge States

So far, the type of boundary conditions we have been using (periodic or magnetic periodic boundary conditions) are used to model systems without boundaries or infinite systems. The Chern number defined is a bulk property, and connected to the Hall conductivity.
In this section, we will relate the Chern number to the number of gap-less edge excitations that exist within the bulk gap when *open boundary conditions* are

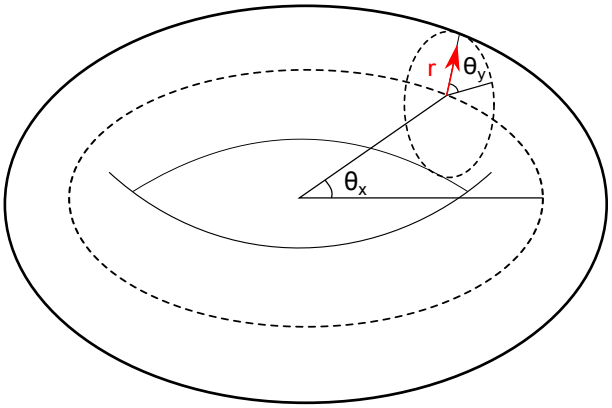

Figure 2.3: Solid torus on which the ground-states are defined on

imposed along one direction, giving the system a strip geometry. The 'edge states' on opposite sides of the system carry current in opposite directions. What the Chern number does is count the number of gap-less edge states on side edge of the strip at each energy in the bulk gap.
A rigorous proof of the statement for a general system is only available for lattice model Hamiltonians and is discussed in [2]. We will provide a short sketch of the proof in the context of continuous systems which we believe holds.
Before showing that, we need to understand that varying the flux parameters is equivalent to varying the boundary conditions while keeping the Hamiltonian fixed. We introduce the so-called 'twisted boundary conditions' where translating over the system size returns the state back to itself with an additional phase factor

$$\begin{aligned} \psi\left(x_1,...,x_i=L_x,...,x_N,\mathbf{y}\right) &= e^{-i\theta_x}\psi\left(x_1,...,x_i=0,...,x_N,\mathbf{y}\right) \quad (2.26)\\ \psi\left(\mathbf{x},y_1,...,y_i=L_y,...,y_N\right) &= e^{-i\theta_y}\psi\left(\mathbf{x},y_1,...,y_i=0,...,y_N\right) \quad (2.27)\end{aligned}$$

then we see that we can either solve for the ground-state of $H\left(\boldsymbol{\kappa}\right)$ in (2.7), under standard periodic boundary conditions, or solve for the ground-state of $H\left(\boldsymbol{\kappa}=0\right)$ under twisted boundary conditions (2.26) and (2.27).
Now we go one step further by introducing a parameter r into the twisted boundary conditions

$$\begin{aligned} \psi\left(x_1,...,x_i=L_x,...,x_N,\mathbf{y}\right) &= e^{-i\theta_x}\psi\left(x_1,...,x_i=0,...,x_N,\mathbf{y}\right) \quad (2.28)\\ \psi\left(\mathbf{x},y_1,...,y_i=L_y,...,y_N\right) &= re^{-i\theta_y}\psi\left(\mathbf{x},y_1,...,y_i=0,...,y_N\right) \quad (2.29)\end{aligned}$$

Clearly $r=0$ corresponds to the specific case of open boundary conditions along y direction. The three parameters (r,θ_x,θ_y) now form a *solid torus*(Fig. 2.3) over which the Berry curvature $\mathcal{F}=-i\mathrm{Tr}\left\{P\left[\partial_{\theta_x}P,\partial_{\theta_y}P\right]\right\}$ is defined at each point. Integrating at constant $r=1$ recovers the bulk Chern number

$$C=\frac{1}{2\pi}\int_0^{2\pi}\int_0^{2\pi}\mathcal{F}\left(r=1,\theta_x,\theta_y\right)d\theta_x d\theta_y \quad (2.30)$$

In [2], the boundary conditions were added as tunneling terms between lattice points at the boundaries of the sample. Hence the flux angles θ_x and θ_y become actual parameters in the Hamiltonian that can be varied, and a Berry Curvature of the ground state can then be associated with them. Here, the Berry Curvature is due to the variation of the ground state due to changes in the boundary conditions.
Now the Berry curvature $\mathcal{F}$ in terms of a Berry connection $\mathcal{A}_\mu$ reads

$$\mathcal{F}\left(1,\theta_x,\theta_y\right)=\left(\frac{\partial\mathcal{A}_y}{\partial\theta_x}-\frac{\partial\mathcal{A}_x}{\partial\theta_y}\right)_{|r=1} \tag{2.31}$$

The fact that the Chern number is non-zero means that $\mathcal{A}_\mu$ cannot be single-valued and smooth on $r=1$ or the integral would vanish via Stokes's theorem. The easiest way to express $\mathcal{A}_\mu$ is to use two overlapping patches. For simplicity, we choose the gauge where

$$\mathcal{A}_x^{(1)}\left(r,\theta,\varphi\right) = -\int_0^{\varphi}\mathcal{F}\left(r,\theta_x,\theta_y'\right)d\theta_y', 0<\theta<2\pi \tag{2.32}$$

$$\mathcal{A}_x^{(2)}\left(r,\theta,\varphi\right) = -\int_{-\pi}^{\varphi}\mathcal{F}\left(r,\theta_x,\theta_y'\right)d\theta_y', -\pi<\theta<\pi \tag{2.33}$$

$$\mathcal{A}_y = 0 \tag{2.34}$$

Then we can write the Chern number as

$$\begin{aligned} C &= \lim_{\epsilon\to 0^+}-\frac{1}{2\pi}\int_{\epsilon}^{2\pi-\epsilon}d\theta_y\int_0^{2\pi}d\theta_x\frac{\partial\mathcal{A}_x^{(1)}}{\partial\theta_y} \\ &= \lim_{\epsilon\to 0^+}-\frac{1}{2\pi}\int_{\epsilon}^{2\pi-\epsilon}d\theta_y\frac{\partial}{\partial\theta_y}\left(\int_0^{2\pi}d\theta_x\mathcal{A}_x^{(1)}\right) \end{aligned} \tag{2.35}$$

if we define

$$\phi\left(r,\theta_y\right) = -\int_0^{2\pi}d\theta_x\mathcal{A}_x^{(1)}\left(r,\theta_x,\theta_y\right) \tag{2.36}$$

$$\Phi\left(r,\theta_y\right) = \exp\left(i\phi\left(r,\theta_y\right)\right) \tag{2.37}$$

then we obtain

$$\begin{aligned} C &= \frac{1}{2\pi}\int_{0^+}^{2\pi^-}d\theta_y\frac{\partial\phi\left(1,\theta_y\right)}{\partial\theta_y} \\ &= \frac{1}{2\pi i}\oint_{r=1}\Phi^{-1}d\Phi \end{aligned} \tag{2.38}$$

So the Chern number becomes a winding number of a $\phi\left(r,\theta_y\right)$ field on the loop $r=1$. Looking back at (2.36), the phase field $\phi\left(r,\theta_y\right)$ is simply the Berry Phase associated with the flux θ_x being varied at constant r and θ_y.
If $C\neq 0$, it means that the phase field ϕ has to have vortex-like singularities within the unit disk $r\in[0,1],\theta_y\in(0,2\pi)$. Since the Berry Phase ϕ is always well defined as long as the ground-state is non-degenerate and separated from the first excited state by a finite energy gap, this means that the singularity has to occur at a point where the ground state acquires degeneracy or the spectrum becomes gap-less.

In [2], it was shown that in general, the point where this singularity occurs need not be at $r = 0$, which corresponds to open boundary conditions. This is because they were working in the setting where at each point in space, there were internal degrees of freedom (e.g. spin, amplitude in different orbitals) for internal generators were introduced that coupled these internal degrees of freedom across the boundary. In the simplified setting above, there were no such internal degrees of freedom, and the singularity point always occurs at $r = 0$.
For a fixed r and θ_x, the parameter θ_y can be put back into the Hamiltonian as a parameter rather than as a parameter in the boundary conditions. Then two Hamiltonians $H(\theta_y)$ and $H\left(\theta'_y\right)$ are unitarily equivalent

$$H\left(\theta'_y\right) = U H(\theta_y) U^\dagger \tag{2.39}$$

$$U = e^{-i\left(\theta'_y - \theta_y\right)\frac{y}{L_y}} \tag{2.40}$$

Therefore, we expect the two spectra of $H(\theta_y)$ and $H\left(\theta'_y\right)$ to be equivalent. If the spectrum were to become gap-less at some non-zero value r_0, this would imply that the spectrum is gap-less for all θ_y, and the phase field ϕ would have a ring of singularities which would give a divergent Chern number. Hence the spectrum has to become gap-less at a single point, and the only possibility is at $r = 0$.

2.5 Relaxing the Constraint of Ground-State Degeneracy and Gapped Spectrum

The arguments above hold whenever the spectrum is gapped, and the many particle ground-state is non-degenerate. This constraint is actually quite a serious one, as it implies that in the non-interacting case, the Fermi energy has to be in an energy gap of the single particle spectrum (or at the bottom of a gap, depending on how we define Fermi energy). This means that perturbations of the Hamiltonian that break these conditions would make the Chern number ill-defined, and the whole idea of a topological invariant that is robust against perturbations would fail.
For non-interacting particles, it can be shown under the framework of *Non-Commutative Geometry* that the requirement for the Fermi energy to be in a gap of the spectrum can be relaxed to the Fermi energy being in a *mobility gap*. Physically, what this means is, as long as the Fermi energy is at a point where the electronic states do not conduct, the Chern number is well defined and robust against perturbations that do not suddenly introduce/remove conducting electronic states, in particular, it is well defined in the presence of spatially homogeneous random disorder where the spectrum could very easily be gap-less, but mobility gaps where only localized states exist due to Anderson localization. The existence of edge states robust against disorder can also be described in such a picture.
The non-commutative Chern number coincides with the Chern number for a clean system defined as an integral over the Brillouin Zone in the absence of disorder. Unfortunately, a full discussion of the mathematical framework is far beyond the scope of this report; we will simply list some of the more recent reviews for the interested reader. [3, 4, 5]

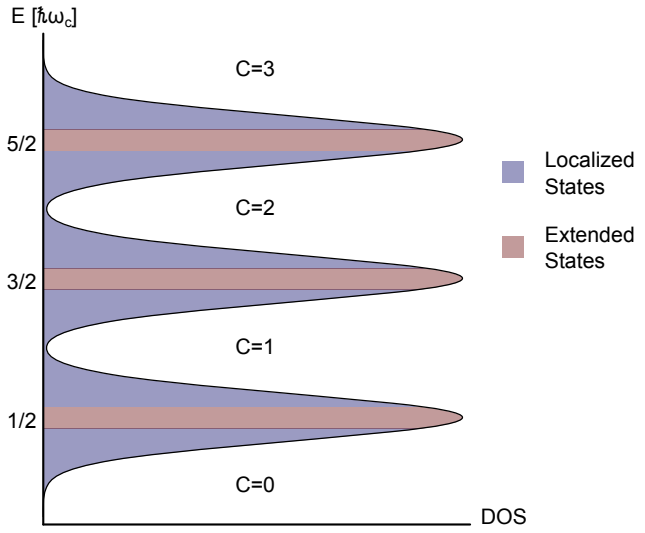

Figure 2.4: Density of States and Chern numbers for IQHE. Chern number is undefined whenever the Fermi Energy is in a region of extended states, but well defined otherwise.

2.6 Examples of Topological Hamiltonians

2.6.1 Integer Quantum Hall Effect(IQHE)

The first example of a Hamiltonian with non-zero Chern number is the integer Quantum Hall effect, or simply, non-interacting charged particles in a uniform magnetic field

$$h(\boldsymbol{\kappa}) = \frac{1}{2m}\left(\mathbf{p} - e\mathbf{A} + \hbar\boldsymbol{\kappa}\right)^2 + V \tag{2.41}$$

V is a possible random disordered potential. In the absence of disorder, the problem can be exactly solved for example, in the Landau gauge $\mathbf{A} = -By\hat{\mathbf{x}}$. Introducing the cyclotron frequency and magnetic length

$$\omega_c = \frac{eB}{n} \tag{2.42}$$

$$l_B = \sqrt{\frac{\hbar}{eB}} \tag{2.43}$$

The result is energy levels(called Landau levels) given by $E_n = \hbar\omega_c\left(n + \frac{1}{2}\right)$. For a system of size L_x, $L_y = p\frac{2\pi l_B^2}{L_x}$, there are p degenerate states for each level n, which gives a degeneracy per unit area equal to $\frac{1}{2\pi l_B^2}$.
In the presence of disorder, the Landau levels are broadened into Landau bands, which comprise of localized states in the band tails. Whenever the Fermi energy lies in a region of localized states, the Chern number is well defined and is equal to the number of Landau levels below the Fermi energy (Fig. 2.4).

2.6.2 Chern Insulators

Chern insulators are a generalization of the IQHE, in the sense that instead of having an infinite number of energy bands, we only consider a n level (band) system in $\mathbf{k}$ space in the clean system limit without disorder. The simplest Chern insulator would be a two-level system in $\mathbf{k}$ where the Hamiltonian is given by

$$h(\mathbf{k}) = \epsilon(\mathbf{k})\mathbb{I} + \mathbf{d}(\mathbf{k}) \cdot \boldsymbol{\sigma} \tag{2.44}$$

where $\boldsymbol{\sigma}$ is the Pauli vector of Pauli matrices. Using (2.25), the Chern number for this system can be computed as

$$C = \frac{1}{4\pi} \int_{BZ} \hat{\mathbf{d}} \cdot \left(\partial_{k_x} \hat{\mathbf{d}} \wedge \partial_{k_y} \hat{\mathbf{d}} \right) d\mathbf{k} \tag{2.45}$$

$\hat{\mathbf{d}} = \frac{\mathbf{d}}{|\mathbf{d}|}$. Chern insulators have not be found experimentally to date; however, *topological insulators* which are just a direct sum of two time-reversed copies of a Chern insulator have been realized experimentally [4].

Chapter 3

Numerical Methods and Models

3.1 Disordered Potentials

The simplest disordered potential would be an additional random on site energy drawn from the interval $\left[-\frac{W}{2}, \frac{W}{2}\right]$, which is the most common form of a disordered potential found in numerical studies. However, one might want to generate a disordered potential with spatial correlations. For completeness, this is discussed in the next section.

3.1.1 Numerical Generation of Correlated Disorder

The goal is to generate a random potential with a particular probability distribution function at a point $D(x)$

$$P(V(\mathbf{r}) = x) = D(x) \tag{3.1}$$

and with an imposed spatial correlation

$$\langle V(\mathbf{r}) V(\mathbf{r}') \rangle = C(\mathbf{r}, \mathbf{r}') \tag{3.2}$$

As we are dealing with a discrete set of grid points, it is more relevant to formulate in terms a discrete field rather than a continuous one, i.e.

$$P(V_i = x) = D(x) \tag{3.3}$$

$$\langle V_i V_j \rangle = C_{ij} \tag{3.4}$$

where each point is labeled by an index. Suppose we begin with generating a set of uncorrelated random numbers with equal variance at a point V_0^2

$$\langle V_i V_j \rangle = V_0^2 \delta_{ij} \tag{3.5}$$

now if we perform a (circular) discrete convolution with some kernel u_i, the

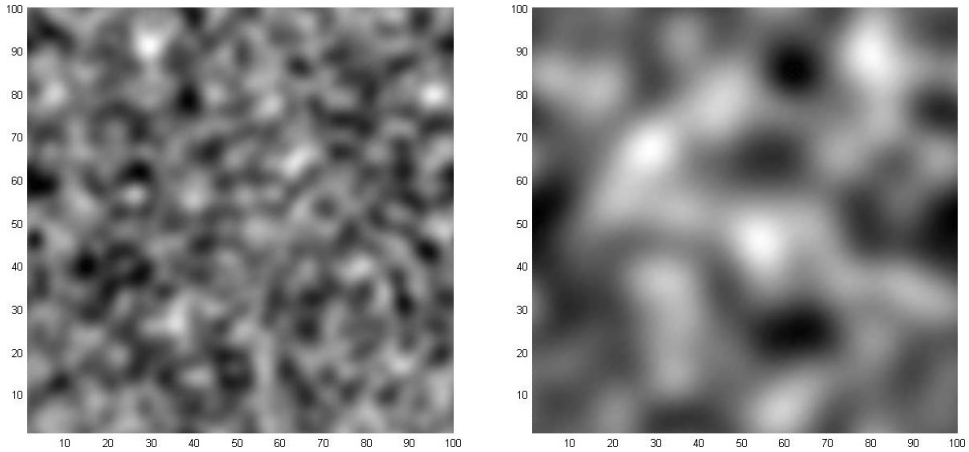

(a) Correlated Disorder with $W_x = W_y = 2$ (b) Correlated Disorder with $W_x = W_y = 5$

Figure 3.1

covariance matrix transforms as

$$\begin{aligned}
\left\langle (V \otimes u)_i (V \otimes u)_j \right\rangle &= \left\langle \left(\sum_{i'=1}^{N} u_{(i-i')} V_{i'} \right) \left(\sum_{j'=1}^{N} u_{(j-j')} V_{j'} \right) \right\rangle \\
&= \sum_{i'=1}^{N} \sum_{j'=1}^{N} u_{(i-i')} u_{(j-j')} \left\langle V_{i'} V_{j'} \right\rangle \\
&= V_0^2 \sum_{i'=1}^{N} \sum_{j'=1}^{N} u_{(i-i')} u_{(j-j')} \delta_{i'j'} \\
&= V_0^2 \sum_{i'=1}^{N} u_{(i-i')} u_{(j-i')} \\
&= V_0^2 \sum_{k=1}^{N} u_{(k)} u_{(j-i+k)} \qquad (3.6)
\end{aligned}$$

where indices in brackets e.g. $(i - i')$ are to be taken modulo N due to circular convolution. This means we can generate a grid of correlated numbers with the desired covariance matrix C_{ij} if the matrix is expressible in terms of a circular autocorrelation of some kernel u_i. It is also clear that if the kernel u_i is normalized such that

$$\sum_{i=1}^{N} u_i u_i = 1 \qquad (3.7)$$

the individual point variance $\langle V_i V_i \rangle$ is preserved.
To efficiently implement convolution numerically, we use FFTs and the convolution theorem. In particular for Gaussian correlated disorder, we consider the

normalized Gaussian kernel

$$\begin{aligned} u(x) &= \frac{1}{\sqrt{\sqrt{\pi}w}} e^{-\frac{x^2}{2w^2}} && (3.8) \\ \tilde{u}(f_x) &= \int_{-\infty}^{\infty} u(x)\, e^{-i2\pi x f_x} dx \\ &= \sqrt{2\sqrt{\pi}w} e^{-2w^2\pi^2 f_x^2} && (3.9) \\ \int_{-\infty}^{\infty} u(x)^2\, dx &= 1 && (3.10) \\ C(x, x') &= V_0^2 e^{-\frac{(x-x')^2}{4w^2}} && (3.11) \end{aligned}$$

which results in a covariance function with correlation length $2w$. The convolution of two functions using Fourier transforms is just the inverse transform of the products of the transforms

$$(g \otimes h)(x) = \mathcal{F}^{-1}\left[\tilde{g}(f_x)\,\tilde{h}(f_x)\right] \tag{3.12}$$

On the grid, the discretized Fourier transform will be given by

$$\tilde{u}_n = \sqrt{2\sqrt{\pi}w} e^{-2w^2\pi^2(n\Delta f_x)^2} \tag{3.13}$$

if we consider the width w in units of the grid spacing Δx,

$$w = W_x \Delta x \tag{3.14}$$

and the fact that the spatial frequency grid spacing is equal to

$$\Delta f_x = \frac{1}{N_x \Delta x} \tag{3.15}$$

we get

$$\tilde{u}_n = \sqrt{2\sqrt{\pi}W_x \Delta x} e^{-2\pi^2\left(\frac{W_x}{N_x}\right)^2 n^2} \tag{3.16}$$

We still need to impose that $\sum_{n=1}^{N_x} u_n u_n = 1$. From the continuous versions, we get

$$\begin{aligned} \frac{1}{N_x}\sum_{n=1}^{N_x} \tilde{u}_n \tilde{u}_n \Delta f_x &= \sum_{n=1}^{N_x} u_n u_n \Delta x \\ &\approx \int_{-\infty}^{\infty} u(x)^2\, dx \\ &= 1 \\ \Rightarrow \sum_{n=1}^{N} \tilde{u}_n \tilde{u}_n &= \frac{1}{N_x \Delta f_x} \\ &= \Delta x \end{aligned}$$

where the first equality follows from the discrete Parseval's theorem for FFTs. Hence the extra factor of Δx in normalization factor for $\tilde{u}_n$ under the root should be removed, and the true frequency transfer function is given by

$$\tilde{u}_n = \sqrt{2\sqrt{\pi}W_x} e^{-2\pi^2\left(\frac{W_x}{N_x}\right)^2 n^2} \tag{3.17}$$

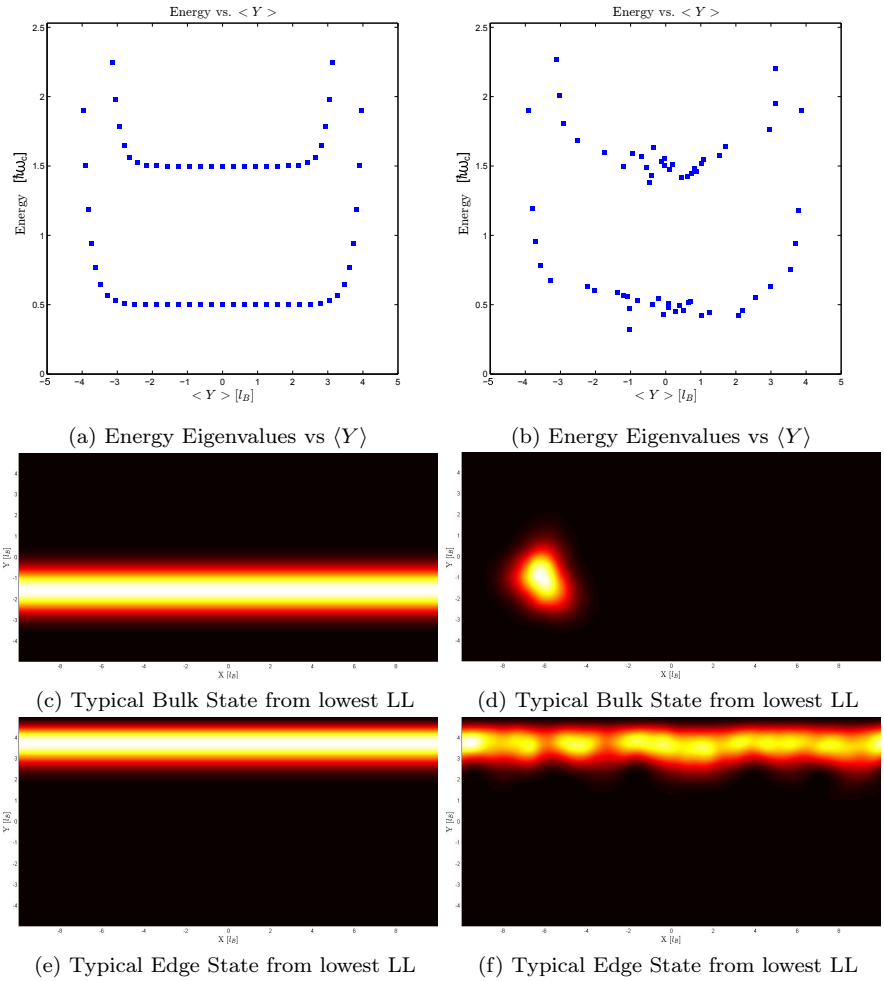

(a) Energy Eigenvalues vs $\langle Y \rangle$

(b) Energy Eigenvalues vs $\langle Y \rangle$

(c) Typical Bulk State from lowest LL

(d) Typical Bulk State from lowest LL

(e) Typical Edge State from lowest LL

(f) Typical Edge State from lowest LL

Figure 3.2: Eigenenergies, Bulk state and Edge State densities, $|\psi(\mathbf{r})|^2$ with (left) and without (right) disorder for IQHE

In summary, firstly, a grid of uncorrelated (Gaussian) random numbers V_n with a particular variance V_0^2 is generated. The FFT of V_n is multiplied by the frequency transfer function $\tilde{u}_n$ and the correlated field is obtained from the IFFT of the product.
Fig. 3.1 shows two examples of correlated disorder generated by this algorithm on a 100 by 100 grid.

3.2 Continuous Model: IQHE

For charged particle in a magnetic field we have the single particle Hamiltonian given by

$$H = \frac{1}{2m}(\mathbf{p} - e\mathbf{A})^2 \tag{3.18}$$

Under the Landau gauge for magnetic field along z direction, $\mathbf{A} = -yB\hat{\mathbf{x}}$. We

obtain

$$\begin{aligned} H &= \frac{1}{2m}\left(-\hbar^2\left(\frac{\partial^2}{\partial x^2}+\frac{\partial^2}{\partial y^2}\right)+(eB)^2 y^2 - i2\hbar eB\frac{\partial}{\partial x}y\right) \\ &= \hbar\omega_c\left(\frac{1}{2}\left(\frac{\partial^2}{\partial X^2}+\frac{\partial^2}{\partial Y^2}\right)+\frac{1}{2}Y^2 - i\frac{\partial}{\partial X}Y\right) \end{aligned} \tag{3.19}$$

where the energy scale is now in units of $\hbar\omega_c$, $\omega_c = \frac{eB}{m}$ and the length scale is in units of the magnetic length $X = \frac{x}{l_B}$, $l_B = \sqrt{\frac{\hbar}{eB}}$.
Using central differences to express the derivatives, i.e.

$$\begin{aligned} \frac{d}{dz}|_{i,i'} &= \frac{\delta_{i+1,i'}-\delta_{i-1,i'}}{2h}+O\left(h^2\right) \\ &= D^z_{i,i'}+O\left(h^2\right) \end{aligned} \tag{3.20}$$

$$\begin{aligned} \frac{d^2}{dz^2}|_{i,i'} &= \frac{\delta_{i+1,i'}-2\delta_{i,i'}+\delta_{i-1,i'}}{h^2}+O\left(h^2\right) \\ &= D^{zz}_{i,i'}+O\left(h^2\right) \end{aligned} \tag{3.21}$$

We have the discretized Hamiltonian as

$$H_{i,i',j,j'} = \hbar\omega_c\left(-\frac{1}{2}\left(D^{xx}_{i,i'}\delta_{j,j'}+\delta_{i,i'}D^{yy}_{j,j'}\right)+\frac{1}{2}Y^2\delta_{i,i'}\delta_{j,j'} - iD^x_{i,i'}Y\delta_{j,j'}\right) \tag{3.22}$$

This four index matrix can then be reshaped and diagonalized numerically on a grid to obtain eigenvectors.
Boundary conditions depend on the matrix terms which join grid points within the grid to points 'outside' of the grid, for example if the number of points along x direction is N_x, given a term δ_{N_x,N_x+1}, the point N_x+1 is not a point on the computational grid. Setting $\delta_{N_x,N_x+1} \to \delta_{N_x,1}$ results in periodic boundary conditions, while setting $\delta_{N_x,N_x+1} = 0$ gives open boundary conditions. From this we can have three different types of geometries:

- Rectangular geometry, where we have open boundaries along both X and Y
- Periodic strip geometry, where we have open boundaries along one direction, and periodic along the other
- Torus geometry, where we have periodic boundaries along both X and Y

In identifying the dominant numerical error term, we note that in the analytical solution for infinite system, the variation along the Y direction is a Hermite polynomial weighted Gaussian, while the variation along the X direction is an oscillating plane wave with wave-number increasing linearly to the edge of the grid. The numerical error stems from taking finite differences, hence we can quantify the error term using the error bound on the approximation of the derivative at the edge of the grid where the variation is the greatest. Hence we expect the numerical error to be dominated by the finite difference approximation along X direction.
In order to get an estimate of the associated numerical error, we use the fact that the analytical solution along the X direction is simply a plane wave. Errors

associated with the central difference approximation are

$$E_1 = -\frac{h^2 f^{(3)}(\xi)}{6} \tag{3.23}$$

$$E_2 = -\frac{h^2 f^{(4)}(\xi)}{12} \tag{3.24}$$

for first and second order derivatives, where ξ is any value in the interval. Since we are considering plane wave behavior, i.e. $f(X) = \exp(ikX)$, the magnitude is bounded by unity, so the upper bound for the absolute errors are

$$E_1 = \frac{h^2 k^3}{6} \tag{3.25}$$

$$E_2 = \frac{h^2 k^4}{12} \tag{3.26}$$

At the edge of the grid, the wave number $k = \frac{L_y}{2}$, and the grid spacing $h = \frac{L_x}{N_x}$ where N_x is the number of grid points along the X direction. Hence we obtain

$$E_1 = \frac{L_x^2 L_y^3}{48 N_x^2} \tag{3.27}$$

$$E_2 = \frac{L_x^2 L_y^4}{192 N_x^2} \tag{3.28}$$

which gives an error estimate in terms of the size of the region and the number of grid points used. It is obvious that the second error term scales very poorly with the size of the system, hence such a continuous model is impractical on very large computational domains.
Fig. 3.2 shows an example of a result using this method, for periodic strip geometry for states close to the first Landau Level. In particular, we see that in the absence of disorder, states in the center of the strip, the bulk states, are just the typical Landau Level(LL) states, that is, localized Gaussians along Y, and plane waves along X with energy eigenvalues $\left(n + \frac{1}{2}\right)\hbar\omega_c$. For states near the edge, the edge states, the energy eigenvalues are found in the gap between LLs. In the presense of disorder with disorder strength $W = 0.5\hbar\omega_c$, and correlation lengths $W_x = W_y = 0.2 l_B$, we see that bulk states no longer behave like plane waves along X. Edge states, however, remain extended along the edge, and retain quasi-plane wave character along X. It should be noted that near the center of the LL, extended bulk states are present, but these do not have plane wave character along X.

3.3 Lattice Model: 1/2 BHZ Chern Insulator

The 1/2 BHZ Model is a Chern insulator model that comes from taking just one spin component of a topological insulator model (the 'full' BHZ-Model). The BHZ model is meant to describe the quantum spin Hall effect in HgTe/CdTe

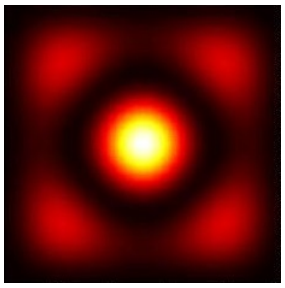

(a) Typical Bulk State, $W = 0$

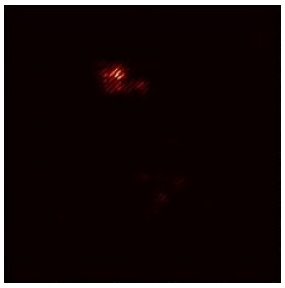

(b) Typical Bulk State, $W = 40$

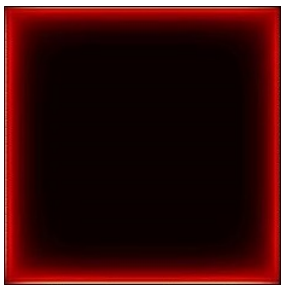

(c) Typical Edge State, $W = 0$

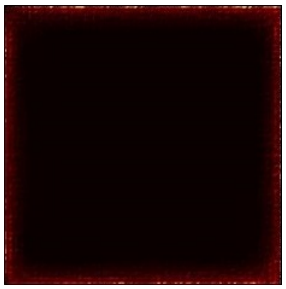

(d) Typical Edge State, $W = 40$

Figure 3.3: Bulk and Edge States $|\psi(\mathbf{r})|^2$ without (left) and with (right) disorder

quantum wells. The Hamiltonian is given by the 4 by 4 matrix[6]

$$
\begin{aligned}
H(\mathbf{k}) &= \begin{pmatrix} h(\mathbf{k}) & 0 \\ 0 & h^*(-\mathbf{k}) \end{pmatrix} && (3.29)\\
h(\mathbf{k}) &= \epsilon(\mathbf{k})\,\mathbb{I} + \mathbf{d}(\mathbf{k})\cdot\boldsymbol{\sigma} && (3.30)\\
\epsilon(\mathbf{k}) &= \frac{D}{a^2}(2 - \cos k_x a - \cos k_y a) && (3.31)\\
\mathbf{d}(\mathbf{k}) &= \begin{pmatrix} \frac{A}{a}\sin(k_x a) \\ \frac{A}{a}\sin(k_y a) \\ M - \frac{2B}{a^2}(2 - \cos k_x a - \cos k_y a) \end{pmatrix} && (3.32)
\end{aligned}
$$

A, B, D, M are model parameters which depend on the width of the quantum well, and a is the lattice constant. The four components of the wavefunction represent the amplitudes in $s_\uparrow, p_\uparrow, s_\downarrow, p_\downarrow$ orbitals respectively. The spin up and down blocks are decoupled and can be solved separately, each describes a Chern insulator, hence the name '1/2 BHZ Model'.
The Hamiltonian $h(\mathbf{k})$ has the following properties.

- There exists a bulk gap of width $2|M|$ at $\mathbf{k} = 0$
- The Chern number when the Fermi energy lies in the bulk gap is

$$
C = \begin{cases} 1 & \text{for } 0 < \frac{M}{B} < 4 \\ -1 & \text{for } 4 < \frac{M}{B} < 8 \\ 0 & \text{otherwise} \end{cases} \qquad (3.33)
$$

The first can be seen from the fact that for any two level system, the energy levels are given by

$$\begin{aligned} E_{\pm}(\mathbf{k}) &= \epsilon(\mathbf{k}) + |\mathbf{d}(\mathbf{k})| \\ \Rightarrow E_{\pm}(0) &= \pm|M| \end{aligned} \tag{3.34}$$

The second can be seen from (2.45). Hence it is the relative sign of M and B that determine whether the system is in a topological phase or not.
In order to introduce boundaries and disorder, we need to transform to real space. In real space representation, h takes the following form

$$h = \sum_{\mathbf{i}} \boldsymbol{\epsilon} c_{\mathbf{i}}^{\dagger} c_{\mathbf{i}} + \sum_{\mathbf{i}} \left(\mathbf{t}_x c_{\mathbf{i}}^{\dagger} c_{\mathbf{i}+\hat{\mathbf{x}}} + \text{H.c} \right) + \sum_{\mathbf{i}} \left(\mathbf{t}_y c_{\mathbf{i}}^{\dagger} c_{\mathbf{i}+\hat{\mathbf{y}}} + \text{H.c} \right) \tag{3.35}$$

$$\boldsymbol{\epsilon} = \begin{pmatrix} -\frac{4(D+B)}{a^2} + M & 0 \\ 0 & -\frac{4(D-B)}{a^2} - M \end{pmatrix} \tag{3.36}$$

$$\mathbf{t}_x = \begin{pmatrix} \frac{(D+B)}{a^2} & -i\frac{A}{2a} \\ -i\frac{A}{2a} & \frac{(D-B)}{a^2} \end{pmatrix} \tag{3.37}$$

$$\mathbf{t}_y = \begin{pmatrix} \frac{(D+B)}{a^2} & \frac{A}{2a} \\ -\frac{A}{2a} & \frac{(D-B)}{a^2} \end{pmatrix} \tag{3.38}$$

where we have expressed h in terms of on-site creation and annihilation operations and matrices that act on the internal degrees of freedom that couple the s and p orbitals.
Open boundary conditions are imposed by truncating the infinite lattice, while periodic boundary conditions are imposed by joining the lattice sites on the edge on the sample to sites on the opposite edge using the matrices $\mathbf{t}_x$ or $\mathbf{t}_y$.
Numerically, we can solve for edge states in the gap and compare them with bulk states. As in the IQHE, the edge states found in the gap remain as quasi-plane waves along the boundary, while bulk states that are initially extended through the sample become localized as shown in Fig. 3.3. In this example, we have used open boundary conditions all around.

Chapter 4

Q-Matrices in Real Space

4.1 Detection of Topological Materials through Conductance Calculations

Although Chapter 2 described the characterization of topological materials through the Chern number, direct calculation of the Chern number is in general not practical numerically. For instance, a naive implementation would require repeated diagonalization of the full Hamiltonian for multiple boundary conditions, from which the projector $P(\theta_x, \theta_y)$ can be calculated as a function of the Fermi energy. For disordered simulations, the results would still require averaging over disorder. Because the computational effort for numerical diagonalization scales with V^3, where V is the volume of the sample, full diagonalization is not a solution as for large samples.
However, due to bulk-edge correspondence, we know that the Chern number gives the number of edge states in the bulk gap along each edge of the sample. Because the counter-propagating edge states exist at the opposite edge of the sample, whenever the Fermi energy lies in the bulk gap, the back scattering is exponentially small for sufficiently wide sample, since in order for the electron to scatter backward, it has to travel across the sample width to the other edge. Since the transmission coefficient for each edge state is perfect, $T = 1$, the Chern number is detected indirectly by calculating conductance and looking for quantized values, for which efficient algorithms exist.

4.2 Q-Matrices

4.2.1 Definition of Proposed Variables

The idea proposed was the following: is there a way to observe a materials topological behavior through the edge states.\? That is, other than measuring conductance, which is somewhat indirect, or direct calculation of the Chern number, which is numerically hopeless for large systems at present, is there another variable that might give us some information on the Chern number? The goal was to obtain characterization of the system only from states that are close to the Fermi energy, instead of all states below Fermi energy.

The proposed variables to study was a set of 2 by 2 matrices which we will call Q-matrices. The inspiration for such a variable comes from the Caroli formula for a two ideal lead conductance measurement[10]

$$G = -\frac{e^2}{h}\mathrm{Tr}\left(\left(\Sigma_L^r - \Sigma_L^a\right) G_{LR}^r \left(\Sigma_R^r - \Sigma_R^a\right) G_{RL}^a\right) \tag{4.1}$$

Here $\Sigma_{L,R}^{r,a}$ are the retarded and advanced self-energies of the left and right leads, and $G^{r,a}$ are the Green's functions connecting the left and right leads. Ignoring the lead self-energies and focusing on the product

$$\begin{aligned} G_{LR}^r G_{RL}^a &= \sum_n \frac{n\left(x_L\right) n^*\left(x_R\right)}{E_F - E_n + i0} \sum_m \frac{m\left(x_R\right) m^*\left(x_L\right)}{E_F - E_m - i0} && (4.2) \\ &= \sum_n \sum_m \frac{\left[n\left(x_L\right) m^*\left(x_L\right)\right]\left[n^*\left(x_R\right) m\left(x_R\right)\right]}{\left(E_F - E_n + i0\right)\left(E_F - E_m - i0\right)} && (4.3) \end{aligned}$$

Here $n\left(x\right) = \langle x|n\rangle$ is the position representation of the nth single particle state. Using

$$\frac{1}{x - x_0 \pm i0} = \mathcal{P}\frac{1}{x - x_0} \mp i\pi\delta\left(x - x_0\right) \tag{4.4}$$

and neglecting the principal value, we get

$$G_{LR}^r G_{RL}^a = \pi^2 \sum_n \sum_m \left[n\left(x_L\right) m^*\left(x_L\right)\right]\left[n^*\left(x_R\right) m\left(x_R\right)\right] \delta\left(E_F - E_n\right) \delta\left(E_F - E_m\right) \tag{4.5}$$

Firstly, the delta functions suggest that only states that are close to the Fermi energy, and also close in energy contribute to the sum. Secondly, we have grouped terms that are different eigenstates evaluated at the same position. Hence the proposed variable to study is the set of 2 by 2 hermitian Q matrices

$$Q_{nm}\left(\mathbf{r}\right) = \begin{pmatrix} n\left(\mathbf{r}\right) n^*\left(\mathbf{r}\right) & m\left(\mathbf{r}\right) n^*\left(\mathbf{r}\right) \\ n\left(\mathbf{r}\right) m^*\left(\mathbf{r}\right) & m\left(\mathbf{r}\right) m^*\left(\mathbf{r}\right) \end{pmatrix} \tag{4.6}$$

that is, matrices formed by pairing up different eigenstates at the same position. When we write $m\left(\mathbf{r}\right) n^*\left(\mathbf{r}\right)$, we mean $\sum_i m_i\left(\mathbf{r}\right) n_i^*\left(\mathbf{r}\right)$, where the sum over i denotes summing over internal degrees of freedom such as spin or orbitals. Since Q_{nm} is hermitian, it can always be parametrized by a unitary matrix

$$\begin{aligned} Q_{nm}\left(\mathbf{r}\right) &= U\left(\mathbf{r}\right) D\left(\mathbf{r}\right) U^\dagger\left(\mathbf{r}\right) \\ U\left(\mathbf{r}\right) &= \begin{pmatrix} \cos\frac{\theta}{2} & i\sin\frac{\theta}{2}e^{-i\chi} \\ i\sin\frac{\theta}{2}e^{i\chi} & \cos\frac{\theta}{2} \end{pmatrix} \end{aligned}$$

that maps $Q_{nm}\left(\mathbf{r}\right)$ to the unit sphere parametrized by $\theta\left(\mathbf{r}\right)$ and $\chi\left(\mathbf{r}\right)$. This is equivalent to writing $Q\left(\mathbf{r}\right) = \epsilon\left(\mathbf{r}\right)\mathbb{I} + \mathbf{d}\left(\mathbf{r}\right)\cdot\boldsymbol{\sigma}$, where $\hat{\mathbf{d}}\left(\mathbf{r}\right)$ would then give the coordinates $\theta\left(\mathbf{r}\right)$ and $\chi\left(\mathbf{r}\right)$ on the unit sphere that $Q_{nm}\left(\mathbf{r}\right)$ has been mapped to.

The question now is where the eigenstates $n\left(\mathbf{r}\right)$ should come from. Since edge states are present whenever a material has non-trivial topology, the proposal was to begin with open boundary conditions on a rectangular sample and look at the behavior of the vector $\hat{\mathbf{d}}$ along the sample boundary for pairs of edge states that are close in energy found in the bulk gap in the presence of disorder. These Q matrices exist in real space unlike the Fermi projector that exists in $\mathbf{k}$ space or (θ_x, θ_y) space.

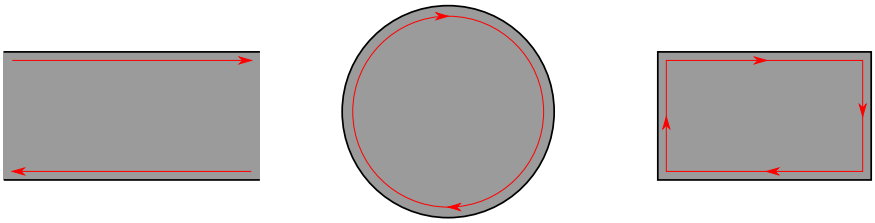

(a) Infinite Strip (b) Finite Disk (c) Finite Rectangle

Figure 4.1: Different Geometries Considered. Arrows indicate edge states. First two have analytic solutions in the clean limit.

4.2.2 Preliminary Problems

The first obvious problem with such a variable is that it is not gauge invariant, multiplying either one of the eigenfunctions by a phase factor $e^{i\delta}$ shifts the angle χ by δ. Hence any physics we hope to obtain from Q_{nm} or equivalently $\mathbf{d}_{nm}$ cannot depend on χ at a particular point in space, but should it exist, must depend on some collective behavior of χ over all the space for example.
Secondly, the Q_{nm} matrix is clearly not basis independent when there are degenerate states. Unitary rotations in a degenerate subspace will produce cross terms in $Q_{nm}(\mathbf{r})$. It is then clear that if there exists any physics related to these variables when degeneracy is present, they have to come from some measure that comes from the collection of all the Q matrices formed from all possible states from the degenerate subspace that is invariant under unitary rotations.
Despite these problems, a study of these variables is still carried out in the next section.

4.3 Results

We study the Q matrices formed from eigenstates of the 1/2-BHZ Chern insulator. For numerical calculations, the following parameters are used

$$\begin{aligned} A &= 364.5 \text{ meV nm} \\ B &= -686 \text{ meV nm}^2 \\ D &= -512 \text{ meV nm}^2 \\ M &= -10 \text{ meV} \end{aligned}$$

which correspond to a Chern number of $C = 1$.

4.3.1 Q-Matrices in the Clean Limit for Exactly Solvable Geometry

Before introducing disorder, we first study the behavior of the Q matrices in the clean limit, for which we have some analytic results. For analytic manipulation,

we consider the small $\mathbf{k}$ approximation (continuum limit) of (3.30).

$$\begin{aligned} h(\mathbf{k}) &= \epsilon(\mathbf{k})\mathbb{I} + \mathbf{d}(\mathbf{k})\cdot\boldsymbol{\sigma} \\ \epsilon(\mathbf{k}) &= -Dk^2 \\ \mathbf{d}(\mathbf{k}) &= \begin{pmatrix} Ak_x \\ Ak_y \\ M - Bk^2 \end{pmatrix} \end{aligned}$$

By making the Peierls substitutions $k_\mu \to -i\partial_\mu$, we can exactly solve the following situations

- Infinite strip geometry $-\frac{L}{2} < y < \frac{L}{2}$
- Finite disk geometry $0 < r < R$

where in accordance with open boundary conditions, the wave function is set to vanish at the boundaries. Analytically, a finite rectangular domain has no closed form solution. A derivation of the eigenstates and eigenenergies can be found in [7, 8]. We simply list the results that are relevant.

1. For infinite strip geometry, k_x is still a good quantum number, and there are two linear dispersions $E_\pm(k_x) = -\frac{MD}{B} \pm \frac{A}{B}\sqrt{B^2 - D^2}k_x$ in the bulk gap that correspond to the edge states on each side of the strip. In particular, at each E, there are two degenerate states propagating in opposite directions, localized spatially at each edge.

2. The edge eigenstates found in the bulk gap for a finite disk geometry take the form $m(r,\varphi) = e^{im\varphi}\begin{pmatrix} \mathcal{N}_m C_m(r) \\ C_{m+1}(r)\, e^{i\varphi} \end{pmatrix}$, and are labeled by an 'angular momentum' index m. Here $C_m(r)$ is some radial function and $\mathcal{N}_m$ is a normalization factor.

3. The energy level spacing for eigenstates on the disk is constant in the large R limit and given by $\Delta E = \frac{A}{B}\sqrt{B^2 - D^2}\frac{1}{R}$. In particular, all states are non-degenerate.

Since we are ultimately interested in studying the behavior on a rectangular finite domain, we focus on the finite disk geometry which resembles this situation the most. Since there is no degeneracy, we can construct the $\mathbf{d}(\mathbf{r})$ vector associated with two arbitrary edge states in the gap without any ambiguity to obtain the following form as a result of point 2.

$$\begin{aligned} \mathbf{d}_{nm}(r,\varphi) &= \begin{pmatrix} F_{nm}(r)\cos(n-m)\varphi \\ F_{nm}(r)\sin(n-m)\varphi \\ G_{nm}(r) \end{pmatrix} \\ F_{nm} &= \mathcal{N}_n C_n(r)\mathcal{N}_m C_m(r) + C_{n+1}(r)C_{m+1}(r) \\ G_{nm} &= \left(\left(\mathcal{N}_n C_n(r)\right)^2 + C_{n+1}(r)^2\right) - \left(\left(\mathcal{N}_m C_m(r)\right)^2 + C_{m+1}(r)^2\right) \end{aligned}$$

Hence at constant $r = r_0$, the $\mathbf{d}_{nm}$ vector precesses $(n-m)$ times about the z-axis as φ goes from 0 to 2π. In particular, we focus on the $\mathbf{d}_{nm}$s that correspond to $(n-m) = 1$, that is, nearest neighbors in energy. The $\mathbf{d}$ vector formed from edge states that are nearest neighbors in energy precess once as we go around the boundary of the sample.

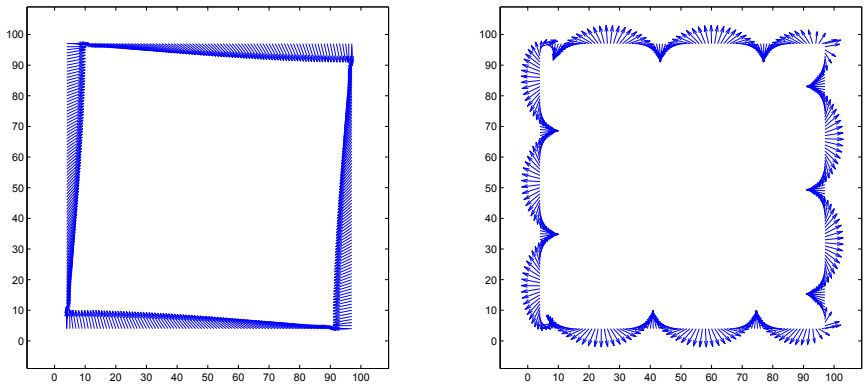

(a) $\mathbf{d}_{nm}$for $n = 1$,$m = 2$ (b) $\mathbf{d}_{nm}$ for $n = 1$,$m = 13$

Figure 4.2: Examples of $\mathbf{d}_{nm}$ precession about sample boundary

4.3.2 Q-Matrices on Rectangular Geometry

For the finite rectangular geometry, we diagonalize the Hamiltonian in (3.30) numerically. In particular we present results for the Q matrices for eigenstates on a square of 100 by 100 lattice points with a lattice constant of $a = 5$nm in the next sections.

4.3.3 Clean Rectangular Geometry

For comparison with the finite disk, these are results for the rectangular geometry without disorder.
Firstly, we numerically obtain 26 eigenstates in the gap. Labeling the eigenfunctions from lowest to highest energy, the energies eigenvalues of the eigenfunctions seem to increase linearly, similar to the case of the disk. Hence it makes sense to label the eigenfunctions with an index n such that energy $E_n \propto n$.
Next, we compute the vector $\mathbf{d}_{nm}$ for pairs of eigenfunctions (n, m). Again, similar to the disk case, $\mathbf{d}_{nm}$ precesses about the z-axis $(n - m)$ as it goes around the boundary of the sample. This is calculated by summing the total precession about the z-axis and divided by 2π, i.e. the winding number about the z-axis. Fig. 4.2 shows some examples of the precession of $\mathbf{d}_{nm}$ for particular pairs of eigenstates.

4.3.4 Disordered Sample

The disorder model used was uncorrelated, uniformly generated random disorder on the interval $\left[-\frac{W}{2}, \frac{W}{2}\right]$. In particular, we calculate the precession of $\mathbf{d}_{nm}$ as a function of E_n and W, for fixed $(n - m) = 1$. Hence, we get a phase diagram in the (W, E_F) plane, that is, in the plane of the energy of one of the eigenstates used to construct $\mathbf{d}_{nm}$, the disorder strength at a fixed level number difference of 1. Fig. 4.3 shows this result, and the phase diagram of the conductance as a function of the Fermi energy and disorder strength, obtained from previous

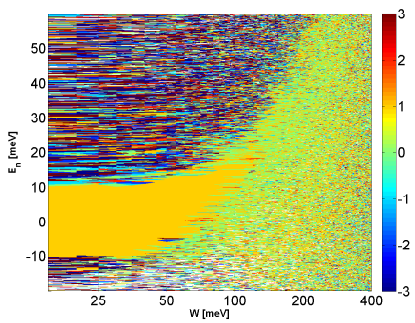

(a) $\mathbf{d}_{nm}$ Precession at fixed $(n-m)=1$ in (W, E_n) Plane

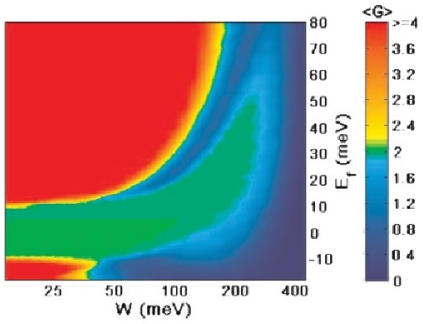

(b) Conductance Phase Diagram in (W, E_F) Plane

Figure 4.3

studies [9]. In other words, we form the Q_{nm} matrices for states which are in general, not edge states when the Fermi energy is not in the bulk gap.

4.4 Remarks and Discussion

The result above is that if we consider only nearest neighbors in energy, then the $\mathbf{d}_{nm}$ vector that characterizes the Q_{nm} matrix formed from these two eigenstates would typically precess around the z-axis once whenever both states are edge states around the boundary of the sample. So it looks as if there is some winding number associated with this vector as we move around the boundary of the sample. There is also some similarities at lower disorder between the phase diagram for the winding number of $\mathbf{d}_{nm}$ and the conductance phase diagram.
The question is whether this number is associated directly with some physical property such as the Chern number, or is simply a re-statement of information that we already know from bulk-edge correspondence. We argue that it is the latter.
Let us look at the Q_{nm} matrix decomposition more carefully. When characterized by the $\mathbf{d}_{nm}$ vector, we decompose the Q_{nm} matrix into components of a

Pauli vector, so

$$\begin{aligned}
\mathbf{d}(\mathbf{r}) &= \frac{1}{2}\begin{pmatrix} Q_{21}+Q_{12} \\ \frac{1}{i}(Q_{21}-Q_{12}) \\ Q_{11}-Q_{22} \end{pmatrix} \\
&= \frac{1}{2}\begin{pmatrix} n(\mathbf{r})\,m^*(\mathbf{r})+m(\mathbf{r})\,n^*(\mathbf{r}) \\ \frac{1}{i}(n(\mathbf{r})\,m^*(\mathbf{r})-m(\mathbf{r})\,n^*(\mathbf{r})) \\ n(\mathbf{r})\,n^*(\mathbf{r})-m(\mathbf{r})\,m^*(\mathbf{r}) \end{pmatrix} \\
&= \begin{pmatrix} \mathrm{Re}\{n(\mathbf{r})\,m^*(\mathbf{r})\} \\ \mathrm{Im}\{n(\mathbf{r})\,m^*(\mathbf{r})\} \\ \frac{1}{2}\left(|n(\mathbf{r})|^2-|m(\mathbf{r})|^2\right) \end{pmatrix} \\
&\equiv d\begin{pmatrix} \sin\theta\cos\chi \\ \sin\theta\sin\chi \\ \cos\theta \end{pmatrix} \\
d &= |\mathbf{d}|
\end{aligned}$$

From which we can see that

$$\begin{aligned}
\tan\theta &= \frac{|n(\mathbf{r})|\,|m(\mathbf{r})|}{2\left(|n(\mathbf{r})|^2-|m(\mathbf{r})|^2\right)} \\
\tan\chi &= \frac{\mathrm{Im}\{n(\mathbf{r})\,m^*(\mathbf{r})\}}{\mathrm{Re}\{n(\mathbf{r})\,m^*(\mathbf{r})\}}
\end{aligned}$$

So the angle θ is simply a measure of the ratio of the products of the amplitudes to the difference of the amplitude squared, while the angle χ is a measure of the phase difference between the two states. This explains the behavior of the angle χ around the boundary when form Q_{nm} from a pair of edge states.
From the infinite strip solution, we know that the edge states behave like quasi one-dimensional channels, so we expect that when we put open boundary conditions all around, only states that obey 1D 'periodic boundary conditions' around the perimeter of the sample will be allowed. So if we define a 'wave-number along the boundary' k, it will be allowed to take values $k = \frac{n2\pi}{P}$, where P is the sample perimeter. From the dispersion relation for the infinite strip, this gives us that $\Delta E = \frac{A}{B}\sqrt{B^2-D^2}\Delta k$. This means that nearest neighbors in energy will simply have a difference of wave-number of one unit. As a result, the total phase difference along the boundary will just be 2π. This argument is consistent with the energy eigenvalues of the finite disk geometry in the continuum approximation.
The next question is why this remains true in the presence of disorder. We use a somewhat semi-classical argument; that is, the length scale at which the random disorder can be resolved by a particular edge state of wave-number k depend on the wavelength associated with that k. Clearly, larger k states will be able to resolve finer details and the reverse for smaller k states. Since the dispersion is linear, this implies that states close in energy are also close in k, so states that are close in energy 'see' the same details in the disordered potential. As eigenstates close in energy are perturbed by the disordered potential in a similar way, this explains why the total phase difference along the boundary between neighboring states is resistant to disorder.

Conversely, if the two states used are both bulk states, or if a bulk state is paired with an edge state, there is no reason to expect any relationship between the phases, hence the total phase difference along the sample boundary looks random in the presence of disorder. In the presence of stronger disorder, the bulk gap vanishes, and there are both edge states and bulk states coexisting at similar energy levels. While coexistence of localized bulk states with extended edge states does not affect the conductance, since localized states simply do not contribute to conductance, the winding number of $\mathbf{d}_{nm}$ is affected severely since it becomes more likely to form 'bulk state-bulk state' pairs or 'bulk state-edge state' pairs as opposed to only 'edge state-edge state' pairs.
Hence we reach the conclusion that the winding of $\mathbf{d}_{nm}$ is simply a restatement that for a non-trivial Chern number, there exist edge states that behave like quasi one-dimensional channels which for this particular model, states close in energy are perturbed in similar ways by the disordered potential due to the linear dispersion. In general, this $\mathbf{d}_{nm}$ winding number does not give the conductance, and hence is not a measure of the Chern number.

Chapter 5

Conclusion

From this perspective, it would seem almost certain that the original Q matrices proposed are not good 'topological variables' to be used in characterizing the conduction properties of a system. Although initially, it seemed that there was some winding number associated with the angle χ, based on the argument presented above, it is most likely a trivial effect due to the behavior of edge states in such materials.
We revisit the original problem: is it possible to obtain the topological number of a system simply by looking at some of the states close to the Fermi energy? This question is clearly self-answering under the case of a restricted bulk-edge correspondence setting, where edge states exist in the energy gap when open boundaries are imposed when the material has non-vanishing Chern number, but do not when the Chern number is zero. The problem then reduces to

1. Look for a bulk gap
2. Are there states in the gap after imposing open boundary conditions? If so, count the number of edge states at each energy to obtain the topological number.

However, the answer is not so clear in the more general setting where the Chern number vanishes in a mobility gap rather than in a gap in the spectrum. In this case there are always states present at all energies, but they are not necessarily conducting. The Q matrices fail to have a winding number in such a regime, where bulk and edge states coexist.
It is then clear that any proposed variable that is local in energy needs to have the following property: it has to give the same results whether the Fermi energy lies in a energy gap or a mobility gap, that is, it must treat localized bulk states as equivalent to having no states at all.

Bibliography

[1] Q. Niu, D. J. Thouless, and Y.-S. Wu, Phys. Rev. B 31, 3372 (1985).

[2] X.-L. Qi, D. Y.-S. Wu, and S.-C. Zhang, Phys. Rev. B 74, 045125 (2006).

[3] Bellissard J, van Elst A and Schulz-Baldes H, J. Math. Phys. 35 5373-5451 (1994)

[4] E. Prodan, J. Phys. A: Math. Theor. 44, 113001 (2011)

[5] E. Prodan, J. Math. Phys. 50, 083517 (2009)

[6] B. A. Bernevig, T. L. Hughes, S.-C. Zhang, Science 314, 1757 (2006)

[7] B. Zhou, H. Z. Lu, R. L. Chu, S. Q. Shen, and Q. Niu, Phys. Rev. Lett. 101, 246807 (2008)

[8] M. Pang, X. G. Wu, arXiv:1309.5559 (2013)

[9] J. Li, R.-L. Chu, J. K. Jain, and S.-Q. Shen, Phys. Rev. Lett. 102, 136806 (2009)

[10] C. Caroli, R. Combescot, P. Nozieres, and D. Saint-James, J. Phys. C 4, 916 (1971)